Supporting Information

Pairwise semi-hydrogenation of alkyne to cis-alkene on platinum-tin intermetallic compounds

Yuchen Pei,[a,†] Minda Chen,[a,†] Xiaoliang Zhong,[b] Tommy Yunpu Zhao,[c] Maria-Jose Ferrer,[c] Raghu V. Maligal-Ganesh,[a] Tao Ma,[d] Biying Zhang,[a] Zhiyuan Qi,[a] Lin Zhou,[d] Clifford R. Bowers,*[c] Cong Liu,*[e] Wenyu Huang*[a,d]

[a.] Department of Chemistry, Iowa State University, Ames, IA 50011, United States

[b.] Huazhong University of Science and Technology, Wuhan, Hubei, China

[c.] Department of Chemistry, University of Florida, Gainesville, FL 32611, United States

[d.] Ames Laboratory, the U.S. Department of Energy, Ames, IA 50011, United States

[e.] Chemical Sciences and Engineering Division, Argonne National Laboratory, 9700 S Cass Ave. Lemont, IL 60439, United States

*corresponding authors: whuang@iastate.edu; congliu@anl.gov; bowers@chem.ufl.edu

[†]These authors contributed equally to this work.

1. Experimental:

Synthesis of Pt@mSiO₂ seeds

The synthesis of Pt@mSiO$_2$ was modified from literature and our previous reports.[1-3] 8.4 g tetradecyltrimethylammonium bromide (TTAB) and 100 mg of potassium tetrachloroplatinate (K$_2$PtCl$_4$) were dissolved in 225 mL water at 50 °C to acquire a transparent solution. 284 mg NaBH$_4$ (in 15 mL cold water) was added to the mixture, and the mixture was maintained at 50 °C for 24 h. Pt nanoparticles were centrifuged at 4000 rpm, 30 min for 4 times to remove large particles, and diluted to 150 mL. 8 mL 0.05 M NaOH aqueous solution was then added to tune pH to 10-11, and 3 mL 10% tetraethyl orthosilicate (TEOS)-methanol solution was added dropwise. The mixture was then stirred at room temperature for another 24 h. The Pt@mSiO$_2$ NPs were separated by centrifugation and redispersed in the solution of 150 mL methanol and 15 mL of a concentrated HCl solution. The Pt@mSiO$_2$ was refluxed at 90 °C for 24 h to remove the surfactant. After methanol wash for 2-3 times, the Pt@mSiO$_2$ was obtained.

Synthesis of PtSn iNPs

The synthesis of PtSn iNPs was modified from our previous reports.[2, 4, 5] 10 mg Pt@mSiO$_2$ seeds were dispersed in 80 mL tetraethylene glycol (TEG) with 11.6 mg SnCl$_2$•2H$_2$O. The mixture was heated to 260 °C in 45 min, and then to 280 °C in 20 min, and maintained at 280 °C for 2 h in Ar under stirring. PtSn iNPs was washed 3 times with ethanol and dried in vacuum.

Synthesis of Pd@mSiO₂ seeds

The synthesis of Pd@mSiO$_2$ was modified from a previous report.[3] 250 μL 10 mM K$_2$PdCl$_4$ aqueous solution was mixed with 450 μL 20 mM NaBH$_4$ aqueous solution, 30 mg TTAB, and 9.3 mL H$_2$O to prepared Pd seed solution. 3 mL of the Pd seed solution was mixed with 20 mL 40 mM ascorbic acid aqueous solution and a pre-mixture of (25 mL 10 mM K$_2$PdCl$_4$ solution, 8.4 g TTAB, 38 mg NaI, and 200 mL H$_2$O). The solution was kept at 60 °C for 3 h with stirring. Pd NPs were centrifuged to remove large particles. The mSiO$_2$ coating process and reflux condition were the same as described for that of Pt analog.

Synthesis of PdCu and Pd₃Sn₂ iNPs

The synthesis of PdCu and Pd$_3$Sn$_2$ follows a similar method as described for the synthesis of PtSn. The seed is Pd@mSiO$_2$, and Cu precursor is CuCl$_2$. The reduction condition is similarly 280 °C for 2 h in Ar under stirring, and all catalysts can be calcined at 500 °C and reduced at 300 °C for the final phase formation.

Synthesis of PtSn/SBA-15 WI control sample

PtSn/SBA-15 WI was prepared by a typical wetness impregnation method. 200 mg SBA-15 powder was dispersed in 10 mL water containing 1 wt.% K_2PtC_4 precursor. After sonicating the mixture for 10 min and evaporating water at 80 °C (overnight), the Pt/SBA-15 was prepared. Pt/SBA-15 was then redispersed in 20 mL acetone and dropwise added 5 mL $SnCl_2 \cdot 2H_2O$-acetone solution maintaining 1:1 Pt/Sn. After evaporating acetone at 40 °C overnight and dried. The powder was reduced in 500 °C for 1 hr under 50 mL/min 10% H_2/Ar to obtain PtSn/SBA-15 WI.

Catalytic reactions for intermetallic compounds

PtSn catalysts were calcined at 500 °C in air for 4 h and reduced at 300 °C for 2 h in 10% H_2/Ar (total flow of 50 mL min^{-1}) before the catalytic evaluation. In a typical reaction of dimethyl acetylenedicarboxylate, 2 mg catalyst was mixed with 20 mg dimethyl acetylenedicarboxylate in 2 mL ethanol, and 20 mg n-decane was added as an internal standard. The reaction was maintained at (110 °C, 5 bar H_2) or (50 °C, 20 bar H_2) in a 4740 Parr high-pressure reactor. Similarly, for the reaction of diphenylacetylene, 2 mg catalyst was mixed with 50 mg diphenylacetylene in 2 mL solvent. 20 mg xylene was added as an internal standard when using toluene as the solvent or 20 mg n-decane as an internal standard when using ethanol as the solvent. The reaction was maintained at 80 °C, 20 bar H_2. For the reaction of 1-phenyl-1-butyne, 5 mg catalyst was mixed with 50 mg 1-phenyl-1-butyne in 2 mL ethanol. The reaction was maintained at 80 °C, 40 bar H_2 for 24 h. Reaction reactants and products were analyzed by an Agilent 6890N/5975 gas chromatograph-mass spectroscopy (GS-MS) equipped with a HP-5ms capillary column (30 m × 0.25 mm × 0.25 μm) and a flame ionization detector (FID). For diphenyl acetylene hydrogenation and 1-phenyl-1-butyne hydrogenation, the conversion of reactant and selectivity of cis/trans-stilbene was analyzed directly in GC-MS. For dimethyl acetylenedicarboxylate, the conversion and chemoselectivity of alkene products were analyzed by GC-MS, and the stereoselectivity of cis/trans-alkene was analyzed by a Bruker 400 MHz NMR. The stereoselectivity of dimethylacetylenedicarboxylate and 1-phenyl-1-butyne hydrogenation semi-hydrogenation is confirmed by NMR with a similar yield as measured by GC-MS.

Characterization

Powder X-ray diffraction (PXRD) patterns were obtained by a STOE Stadi P powder diffractometer with Cu K_α radiation (40 kV, 40 mA, λ = 0.1541 nm). Extended X-ray absorption fine structure spectroscopy (EXAFS) and X-ray absorption near-edge spectroscopy (XANES) spectra were acquired in transmission mode at 9-BM-B and 20-BM-B beamlines of the Advanced Photon Source in Argonne National Laboratory (Pt L_3 edge = 11564 eV and Sn K edge = 23220 eV). EXAFS of reference samples

were collected using pure metal foils. The Athena program, which is an interface to IFEFFIT and FEFFIT, was used for raw data processing. All the EXAFS data were fitted with k^3 weight in R space by Artemis program from the same package using the quick shell theory.

2. Structural clarification of PtSn iNPs

The structure of PtSn was clarified with extensive characterizations in our previous reports, including ICP-MS, HAADF-STEM, EDS mappings, XPS, AP-XPS, PXRD, EXAFS, and CO-DRIFTS studies.[2, 4, 5] In short, these PtSn iNPs have highly ordered structures in both bulk and surface matching to their theoretical model of intermetallic PtSn without the presence of Pt three-fold sites. The ICP-MS result shows the Pt/Sn ratio of 0.99 ± 0.04.[4] The HAADF-STEM image and EDS mappings demonstrate the atomic ordering of PtSn single-crystal phase through single particles with uniform Pt and Sn signals.[2, 5] AP-XPS results show the Pt/Sn ratios of 0.91, 0.91, and 0.94 in as-synthesized, 300, and 500 °C reduced samples, indicating a stable Pt/Sn ratio under reductive environments in agreement with the theoretical Pt/Sn ratio (1:1).[5] In Pt L$_3$ edge, EXAFS fittings show the Pt-Pt coordination number of 2.1(0.4), and Pt-Sn coordination number of 3.6(0.2).[4] In Sn K edge, EXAFS fittings show the Sn-Pt coordination number of 6.4(1.1).[4] These fittings are close to the theoretical Pt-Pt, Pt-Sn, and Sn-Pt coordination number of 2, 6, and 6 in intermetallic PtSn crystals. CO-DRIFTS studies also show only one mode of atop Pt (2060 cm^{-1}), and the mode of Pt multi-sites was not observed.[5] In comparison, Pt shows two modes of atop Pt (2072 cm^{-1}) and Pt multi-sites (1854 cm^{-1}), demonstrating the abundant surface Pt three-fold sites.[5] The absence of Pt three-fold sites feature over PtSn iNPs was also confirmed by the signal enhancement in PHIP-NMR studies (w/ propene hydrogenation)[6] with the similar experiments and concept as described in the below section of 1-phenyl-1-butyne hydrogenation.

3. Structural clarification of PtSn iNPs vs. PtSn impregnated samples

To better illustrate the structure difference of PtSn iNPs, we prepared PtSn impregnated samples by supporting PtSn small nanoparticles on SBA-15 (denoted as PtSn/SBA-15 WI). PtSn/SBA-15 WI has uniform particles with size ranging from 6-10 nm, and PXRD shows the formation of the intermetallic PtSn phase. However, the EXAFS data of PtSn/SBA-15 WI tells that the impregnated sample has significantly higher Pt-Pt CNs and lower Pt-Sn CNs in comparison to PtSn iNPs. PtSn/SBA-15 WI has more Pt cluster structure (even not visible in PXRD) in comparison to the very uniform structure of PtSn iNPs. In this comparison, PtSn iNPs show exclusively accurate structure reflecting the theoretical PtSn intermetallic compound other than the general impregnated catalyst.
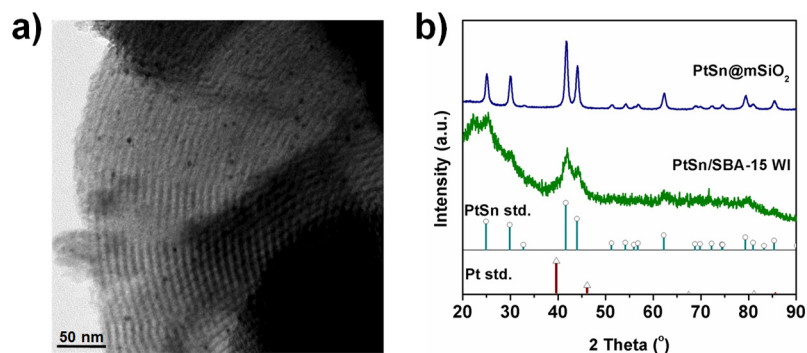
Figure S1. **a**) TEM image of PtSn/SBA-15 WI with ~ 5 nm bimetallic particles; **b**) PXRD patterns of PtSn@mSiO$_2$ and PtSn/SBA-15 WI. Both of two spectra agree with that of characteristic intermetallic PtSn standard.
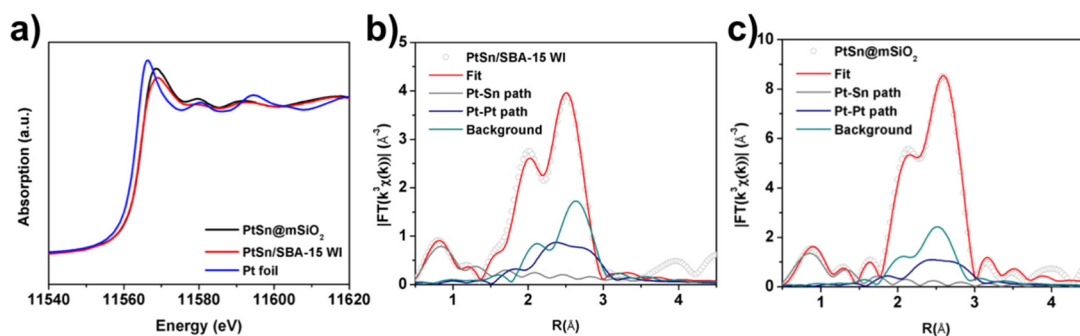

Figure S2. **a**) Normalized X-ray absorption near edge structure (XANES) spectra of Pt L$_3$ edge in PtSn@mSiO$_2$, PtSn/SBA-15 WI, and Pt foil. PtSn@mSiO$_2$ and PtSn/SBA-15 WI have similar whiteline energy that positions at higher energy than that of Pt foil. **b**) and **c**) are respective fitting results of EXAFS data for PtSn@mSiO$_2$ and PtSn/SBA-15 WI. R range = 1.5-11.5; k range = 2.2-11.8, k^3-weight.

Table S1. EXAFS fitting summary of Pt L_3 edge in PtSn@mSiO$_2$ and PtSn/SBA-15 WI.[a]

Entry	PtSn@mSiO$_2$	PtSn/SBA-15 WI
Pt-Pt coordination number	2.1(0.4)	2.9(0.3)
Pt-Pt bond distance (Å)	2.74	2.74
Pt-Sn coordination number	4.6(0.2)	2.9(0.2)
Pt-Sn bond distance (Å)	2.72	2.70
Energy shift (eV)	4.9(0.2)	-10.2(1.3)
Del(r) (Å)	0.016(0.005)	0.04(0.01)
Delby-Waller factor	define as 0.006	define as 0.007
R factor	0.00004	0.0005

a. R range = 1.5-11.5; k range = 2.2-11.8, k^3-weight. The fitting uses quick shell theory.

4. The function and blockage of mesoporous silica shell in PtSn iNPs

The mesoporous silica shells prevent the encapsulated bimetallic particle from aggregation at high-temperature/long-time annealing. The high thermostability of these individually encapsulated bimetallic nanoparticles allows us to convert them into ordered intermetallic structures regardless of concerns in compositional heterogeneity due to the catalyst sintering. The mesoporous silica shells have uniform pore sizes of 2.5-2.8 nm, which allows the access of most of the small molecules as studied in our previous reports (nitrobenzene, nitrostyrene, and furfuryl).[2, 3, 5]

The use of mesoporous silica will partially block surface active sites. The Pt dispersion is measured as 6.5% by CO chemisorption,[2, 4] which is lower than the theoretical value (10%) for 14 nm Pt NPs (estimated by using spherically shaped particles covered solely by Pt(111) facets), giving a corrector factor of 0.65 due to the blockage of mesoporous silica shells. For PtSn iNPs, the dispersion is measured as 1.8%, which is close to the calculated value of 2.2% considering the corrector factor due to the mesoporous silica shell blockage.[2, 4]

The theoretical dispersion of PtSn iNPs is calculated to be 6.8%. The surface of PtSn is covered by only 50% of Pt atoms and applied the corrector factor of 0.65. The corrected fraction of exposed Pt sites is then 2.2%. The theoretical fraction (6.8%) of Pt atom sites on PtSn surface is estimated from the equation (*Langmuir*, **1997**, 13, 5613): *Dispersion = 5.01D_{at}/D = 6.8%,* where D_{at} is the average diameter of Pt/Sn atoms (0.273 nm), D is the PtSn particle size (20 nm), and dispersion is defined as the fraction of exposed surface atoms of both Pt and Sn.

5. Structural characterization of PdCu and Pd$_3$Sn$_2$ iNPs

PdCu and Pd$_3$Sn$_2$ iNPs have bulk structures agreeing to their structural models, as evidenced by ICP-MS analysis and PXRD patterns.

Table S2. ICP-MS result of PtSn, PdCu, and Pd$_3$Sn$_2$.

Intermetallic compound	Metal ratio
PtSn	Pt:Sn = 1.0:1
Pd$_3$Sn$_2$	Pd:Sn = 1.2:1
PdCu	Pd:Cu = 1.0:1
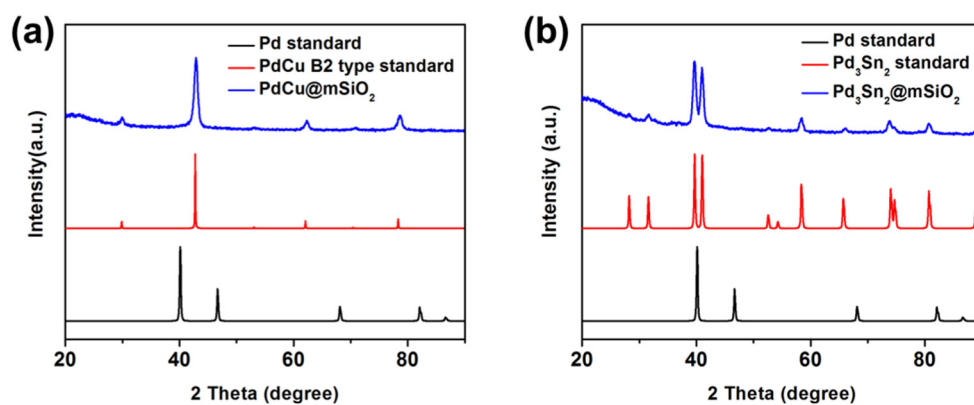
Figure S3. XRD patterns of **a**) PdCu, and **b**) Pd$_3$Sn$_2$.
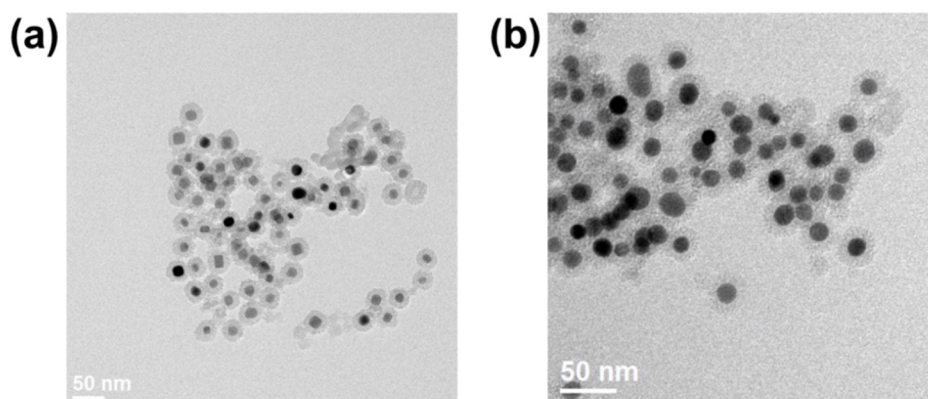
Figure S4. TEM images of **a**) PdCu, and **b**) Pd$_3$Sn$_2$.
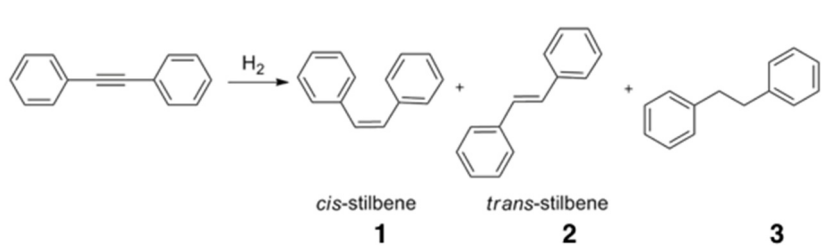
6. Supplementary catalytic results

Table S3. Semi-hydrogenation of dimethyl acetylenedicarboxylate over Pt and PtSn catalysts.
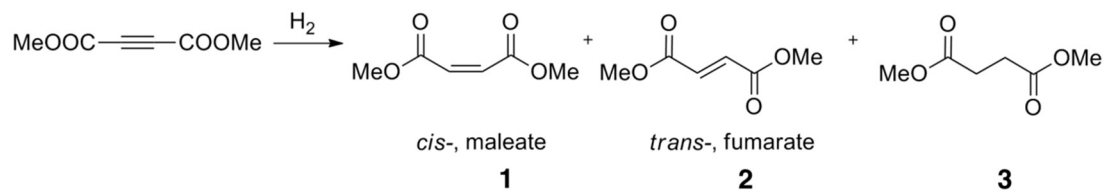
Catalyst	T (°C)	Time (h)	Conversion (%)	Chemoselectivity (%)		Stereoselectivity (%)	
				1+2, C=C	3, C–C	1, *cis-*	2, *trans-*
Pt	50	0.5	42.9	67.0	33.0		—
	50	1	>99	36.3	63.7	33.0	67.0
PtSn	50	16	12.4	87.9	12.1	>99	—
	110	3	9.4	91.2	8.8	>99	—
	110	18	79.8	82.7	17.3	>99	—

Reaction condition: 2 mg catalyst, 20 mg dimethyl acetylenedicarboxylate, 2 mL ethanol, 20 mg n-decane as an internal standard, 110 °C, 5 bar H_2 or 50 °C, 20 bar H_2.

Table S4. Semi-hydrogenation of diphenylacetylene over Pt and PtSn catalysts.

Catalyst	Time (h)	T (°C)	Solvent	Conversion (%)	Chemoselectivity (%)		Stereoselectivity (%)	
					1+2, C=C	3, C–C	1, *cis-*	2, *trans-*
Pt	0.5	50	ethanol	14.4	>99.9	0	86.4	13.6
	1	50	ethanol	28.0	>99.9	0	86.1	13.9
	3	50	ethanol	70.5	>99.9	0	84.4	15.6
	6	50	ethanol	> 99	6.2	93.7	0	>99.9
PtSn	2	80	toluene	17.8	>99.9	0	>99.9	0
	16	50	ethanol	25.8	>99.9	0	>99.9	0
	12	80	toluene	93.1	>99.9	0	91.2	8.8
	35	80	toluene	>99	>99.9	0	83.4	16.6

Reaction condition: 2 mg catalyst, 50 mg diphenylacetylene, 2 mL solvent, 20 bar H_2, and 20 mg xylene (n-decane) as an internal standard when toluene (ethanol) is used as the solvent.

Table S5. Catalytic results of 1-phenyl-1-butyne hydrogenation over PtSn iNPs.
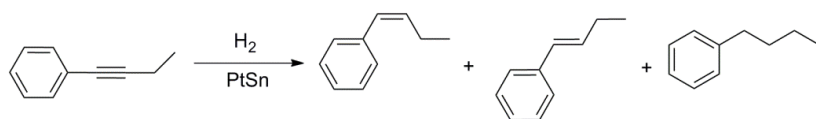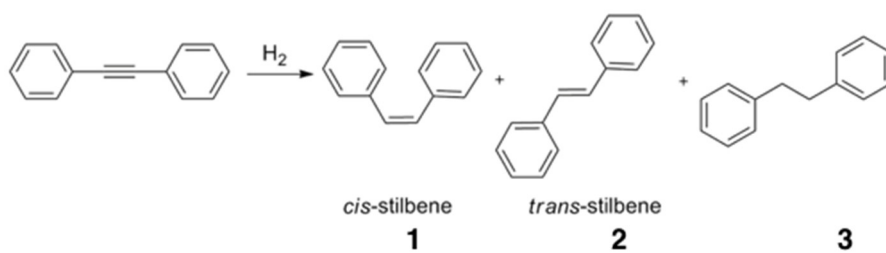

catalyst	time (h)	conversion (%)	Chemoselectivity (%)		Stereoselectivity (%)	
			1+2, C=C	3, C–C	1, *cis-*	2, *trans-*
Pt	3	84	53.3	46.7	80.3	19.7
	12	99.7	30.6	69.4	0	>99.9
PtSn	24	67.4	97.6	2.4	85.8	14.2

Reaction condition: 10 mg Pt catalyst or 20 mg PtSn catalyst, 50 mg 1-phenyl-1-butyne, 2 mL ethanol, 80 °C, 40 bar H_2, 24 h.

**Table S6**. Catalytic results of cis-stilbene spontaneous isomerization over PtSn.
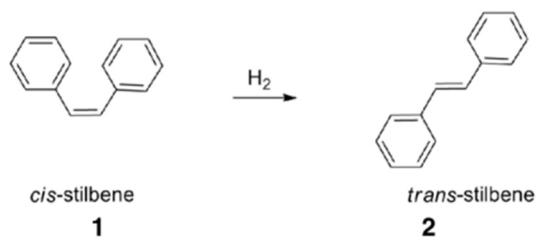
catalyst	time (h)	temperature (°C)	conversion (%)
PtSn	23	60	-
	15	80	-
Blank, no catalyst	23	60	-
	15	80	-

Reaction condition: 2 mg catalyst, 50 mg cis-stilbene, 2 mL toluene, 20 mg xylene, 20 bar H_2.

Table S7. Catalytic results of diphenyl acetylene hydrogenation on $Pt_{1.0}Sn$ and $Pt_{1.1}Sn$.

catalyst	time (h)	conversion (%)	Chemoselectivity (%)		Stereoselectivity (%)	
			1+2, C=C	3, C–C	1, *cis-*	2, *trans-*
$Pt_{1.0}Sn$	3	29.3	>99.9	0	91.4	8.6
	6	55.6	>99.9	0	93.3	6.7
	12	93.1	>99.9	0	91.2	8.8
	35	>99	>99.9	0	83.4	16.6
$Pt_{1.1}Sn$	3	24.5	>99.9	0	90.0	10.0
	6	43.5	>99.9	0	91.2	8.8
	12	69.5	>99.9	0	91.7	8.3
	35	>99	>99.9	0	64.6	35.4

Reaction condition: 2 mg catalyst, 50 mg diphenyl acetylene, 2 mL toluene, 20 mg xylene, 80 °C, 20 bar H_2.

Table S8. Catalytic results of diphenyl acetylene hydrogenation over PdCu and Pd$_3$Sn$_2$.
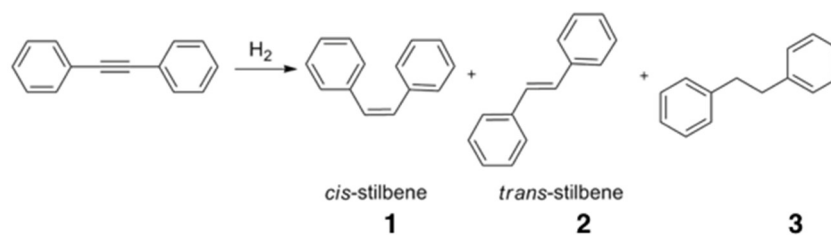
catalyst	time (h)	conversion (%)	Chemoselectivity (%)		Stereoselectivity (%)	
			1+2, C=C	3, C–C	1, *cis-*	2, *trans-*
PdCu	1	97.5	47.2	52.8	>99.9	0
	3	>99	0	>99.9	-	-
Pd$_3$Sn$_2$	1	23.1	>99.9	0	89.2	10.8
	3	41.1	>99.9	0	92.2	7.8
	6	54.0	>99.9	0	92.9	7.1
	12	64.0	>99.9	0	93.2	6.8
	35	78.1	>99.9	0	92.5	7.5

Reaction condition: 2 mg catalyst, 50 mg diphenyl acetylene, 2 mL toluene, 20 mg xylene, 80 °C, 20 bar H$_2$.
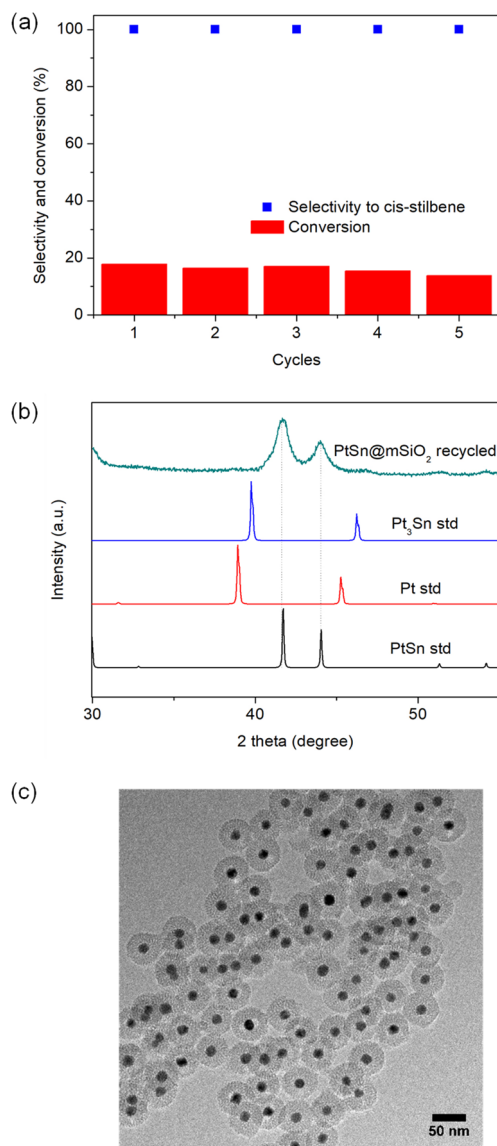
Figure S5. (a) Recycle test of PtSn@mSiO$_2$ with diphenylacetylene hydrogenation. (b) XRD and (c) TEM characterization of the catalyst after 5 cycles.

Table S9. Recent catalysts reported in literature for the semi-hydrogenation of diphenylacetylene.

Catalyst	conversion (%)	chemoselectivity (%)	stereoselectivity (%)	reference
PtSn@mSiO$_2$	>99	>99.9	83.4	This work
Pd/CeO$_2$	~100%	~80	~93	ChemCatChem, 2015, 7, 952
PdIn/α-Al$_2$O$_3$	~100%	~85	~94	Nanomaterials, 2018, 8, 769
Pt/SiO$_2$	99	77	91	ACS Catal., 2014, 4, 10, 3581
Rh/SiO$_2$	99	41	54	ACS Catal., 2014, 4, 10, 3581
Rh$_2$Sb/SiO$_2$	99	94	40	ACS Catal., 2014, 4, 10, 3581
Pd-HAS	93	95	96	ACS Catal., 2013, 3, 8, 1700
Ni@CNTs	100	100	94	Chem. Commun., 2017, 53, 7894

7. Structural clarification of $Pt_{1.1}Sn$ iNPs

The structure of $Pt_{1.1}Sn$ was clarified with detailed characterization by ICP-MS, PXRD, EXAFS, and CO-DRIFTS studies in our previous report.[4] The Pt contiguous sites were observed in both bulk and surface of $Pt_{1.1}Sn$ iNPs. The $Pt_{1.1}Sn$ iNPs likely have structures of PtSn cores with Pt-rich PtSn shells. The Pt/Sn ratio was determined by ICP-MS to be 1.16 ± 0.03.[4] The PXRD pattern of $Pt_{1.1}Sn$ iNPs shows the presence of Pt monometallic peaks due to the presence of monometallic Pt cores, which agrees to the EXAFS, EDS mappings, and line scan results.[4] The surface of $Pt_{1.1}Sn$ iNPs is likely Pt-rich PtSn, which is evidenced by the CO-DRIFTS analysis and two probe reactions with consistent results similar to that of monometallic Pt control.[4]

8. PHIP-NMR analysis details

The pairwise stereoselective hydrogenation of the PtSn@mSiO$_2$ iNPs in the semi-hydrogenation of alkyne substrate over the PtSn catalyst was demonstrated in the hydrogenation of 1-phenyl-1-butyne with 50% parahydrogen. The apparatus for parahydrogen enrichment and bubbling of the gas through the suspensions containing the dissolved substrate and catalyst is described in Ref. 6. Spectra were collected on a Varian Mercury NMR Spectrometer operating at 300 MHz. In this experiment, 0.6 mL of 100 mM 1-phenyl-1-butyne in d$_6$-acetone and 15mg of PtSn@mSiO$_2$ iNPs (12nm) were added to a modified 5 mm NMR tube and pressurized to 7 bars. The bubbling of the hydrogen through the reaction mixture was controlled in the NMR pulse program by activating the TTL-controlled solenoid valves. Each cycle of the PASADENA experiment consisted of (1) 20s of bubbling with parahydrogen, (2) a delay of 1s before allowing the hydrogen bubbles to subside, and (3) acquisition of the free induction decay using a single $\pi/4$ radiofrequency pulse. The signal enhancement (SE) was calculated by dividing the area of the absorptive component of the PASADENA multiplet (δ=6.42 ppm) by the change in the area of the thermally polarized peak, which is proportional to the amount of alkene formed during the same bubbling cycle. To correct the SE for the intensity loss due to the substantial destructive interference between the absorption and emission components of the PASADENA antiphase signal pattern, deconvolution lineshape fitting, as shown in Figure S5, was carried out to estimate the area of the absorptive component of the PASADENA antiphase signal, S_{ads}, for proton #1 of cis-1-phenyl-1-butene. The signal enhancement of the cis-1-phenyl-1-butene product was estimated using the following formula:

$$SE = \frac{S_{ads} - \Delta S_{therm}/n}{\Delta S_{therm}/n}$$

where ΔS_{therm} is the change of the area of the CH peak of cis-1-phenyl-1-butene in the thermally polarized spectrum after the parahydrogen bubbling, n is the number of FID's acquired and co-added to obtain the thermally polarized spectrum ($n = 32$ in this experiment).
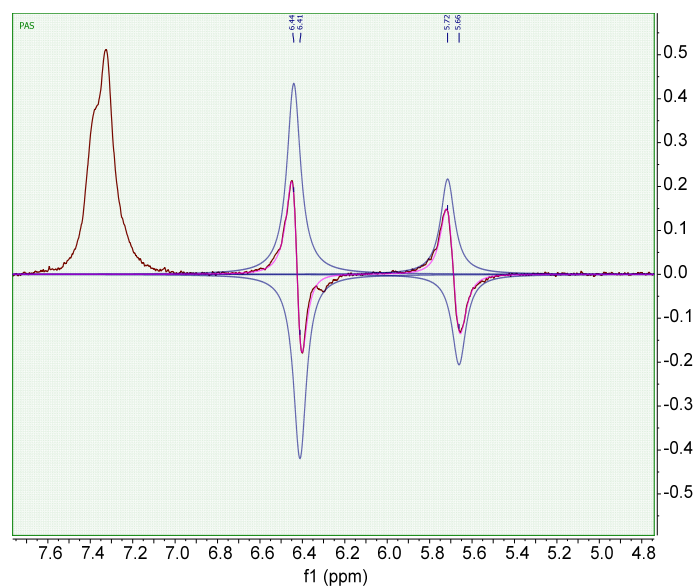
Figure S6. Deconvolution of the antiphase multiplets into absorptive and emissive components, allowing the underlying peak areas to be determined.

The accumulation of alkene product after one to six bubbling cycles can be seen in Figure S7
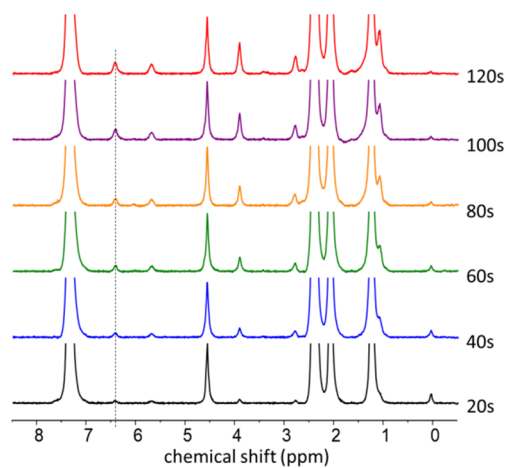

Figure S7. Thermally polarized spectra obtained after integral multiples of 20 s of bubbling. These spectra were collecting after bubbling n-H_2 through the catalyst slurry. Each spectrum represents the accumulation of 32 transients using a 10 s recycle delay and a $\pi/2$ RF pulse.

9. Computational details

The DFT calculations are performed via the Vienna ab initio simulation package (VASP),[7] with ion-electron interaction described by the projector augmented wave (PAW) method.[8] Electron exchange-correlation is represented by the functional of Perdew, Burke, and Ernzerhof (PBE) of generalized gradient approximation (GGA).[9] To improve the description for inter-molecular noncovalent interactions between adsorbed molecules and metal surfaces, the DFT-D3 method of Grimme is applied.[10] The cutoff energy of the plane-wave basis set is 400 eV. All modeled metal surfaces are along the z-direction with about 10 Å of vacuum. The k-point sampling for all the surface systems is performed by a (2x2x1) mesh within the Monkhorst-Pack scheme,[11] and Γ-point is used for all the isolated molecules. The following surfaces are studied: (111) for Pt with a (6x6) lateral cell, (110) for PtSn with a (4x2) cell, and (001) for Pd_3Sn_2 with a (4x4) cell and (100) for Pd_2Sn with a (4x3) cell. The surface atoms are relaxed with residual forces smaller than 0.05 eV/Å.

Table S10. Summary of diphenylacetylene and diphenylethylene adsorption energies over Pt and intermetallic surfaces.

	structure	$E_b(Ph_2C_2)$	cis←$E_b(Ph_2C_2H_2)$→trans	
Pt	111	-3.17	-3.12	-2.45
PtSn	110	-1.31	-1.36	-0.49

Table S11. Summary of H_2 dissociation energies on Pt and intermetallic surfaces.

	structure	$E_b((H_2 + * \rightarrow H_2*))$	barrier$\Delta E^\ddagger$ ($H_2* \rightarrow$ 2H*)	$\Delta E(H_2* \rightarrow 2H*)$
Pt	111	-0.022	0	-1.014
PtSn	110	-0.052	0.26	-0.615

E_b is the binding energy, with the sum of energy of isolated surface and H_2 molecule taken as zero energy. "*" denotes a surface binding site.
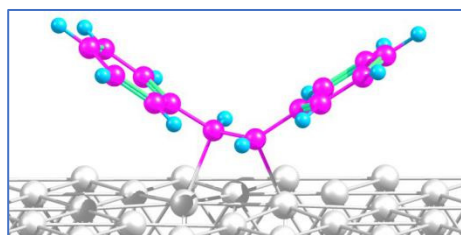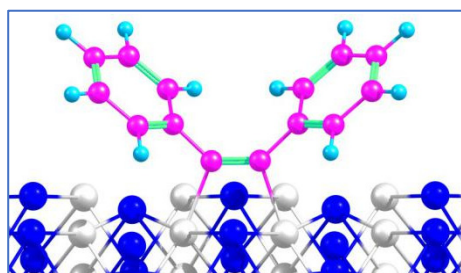
Pt
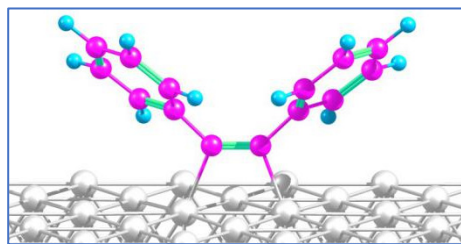
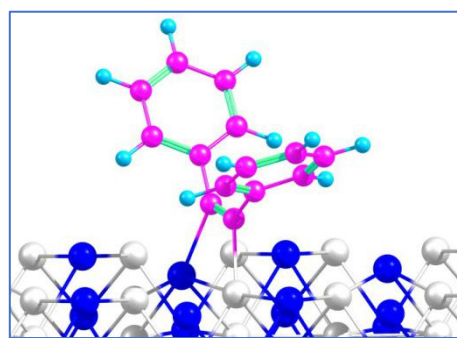Pt-Ph$_2$C$_2$ (-3.17 eV)
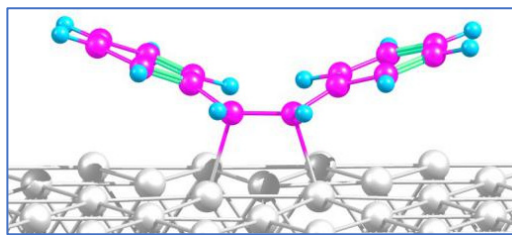
Pt-cis (-3.12 eV)

Pt-trans (-2.45 eV)

Figure S8. Calculated molecular configurations of diphenylacetylene and diphenylethylene over metallic Pt. Pt in grey atoms, C in purple, and H in cyan atoms.
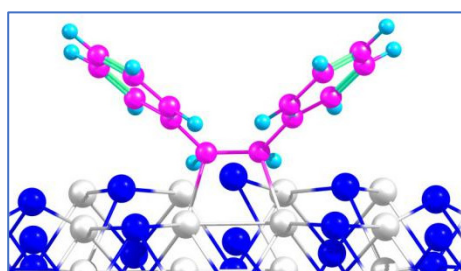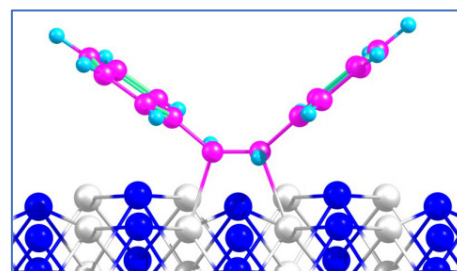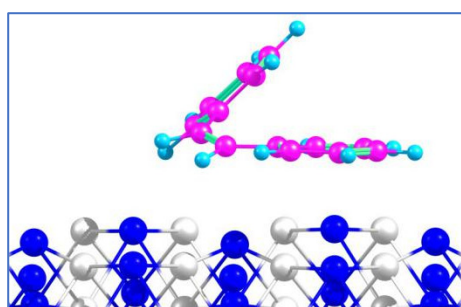
PtSn(Pt&Pt)-Ph2C2 (-1.31 eV)
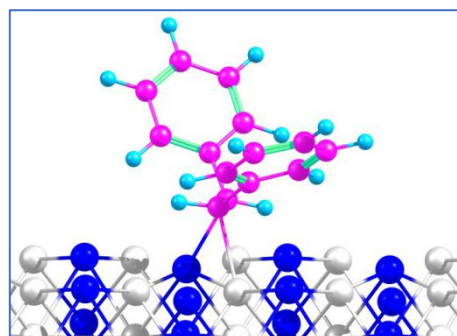
PtSn(Pt&Sn)-Ph2C2 (-0.96 eV)

PtSn(Pt&Pt)-cis (-0.68 eV)

PtSn(Pt&Pt)-trans (-0.33 eV)

PtSn(Pt&Sn)-cis (-1.36 eV)

PtSn(Pt&Sn)-trans (-0.49 eV)

Figure S9. Calculated molecular configurations of diphenylacetylene and diphenylethylene over PtSn. Pt in grey, Sn in dark blue atoms, C in purple atoms, and H in cyan atoms.
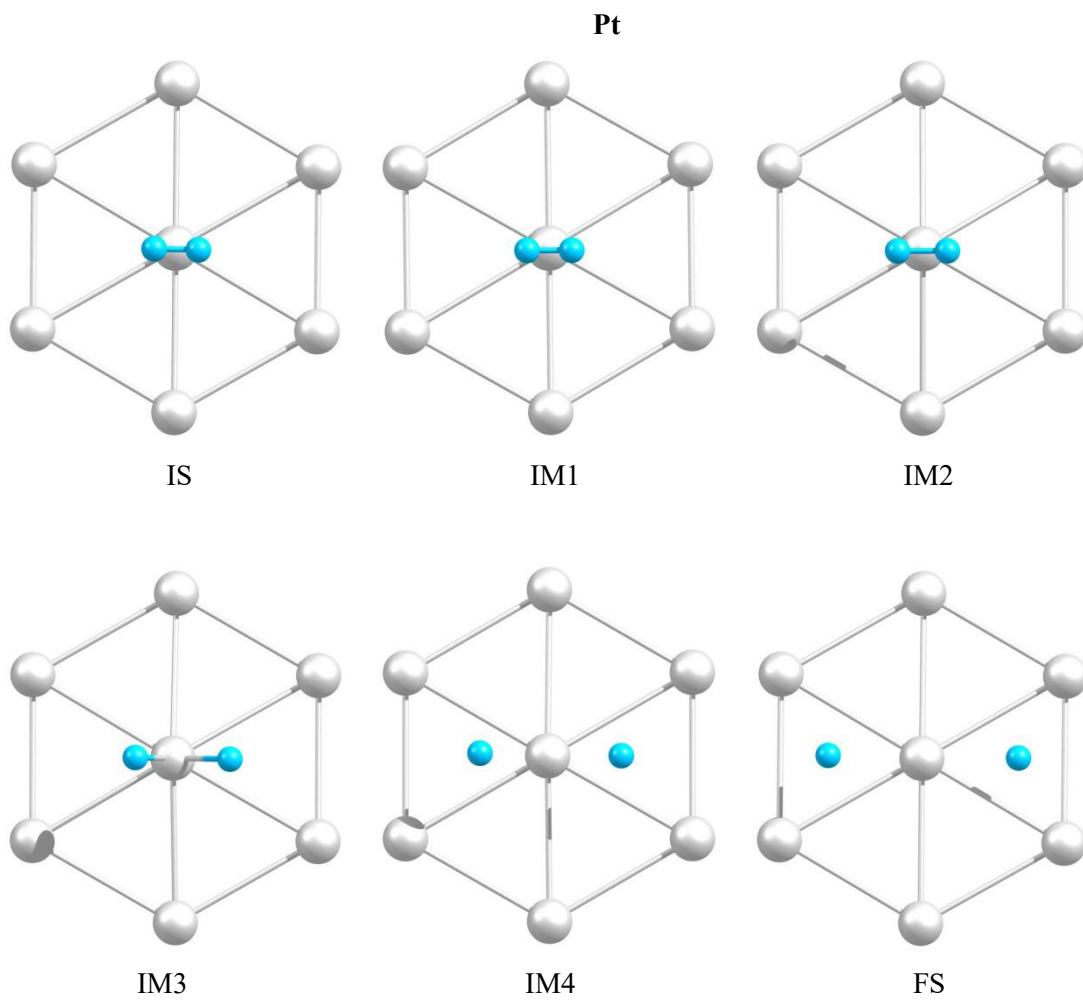
Pt

IS	IM1	IM2

IM3	IM4	FS

Figure S10. Calculated molecular configurations of molecular H_2 over metallic Pt. Pt in grey atoms, and H in cyan atoms.

PtSn

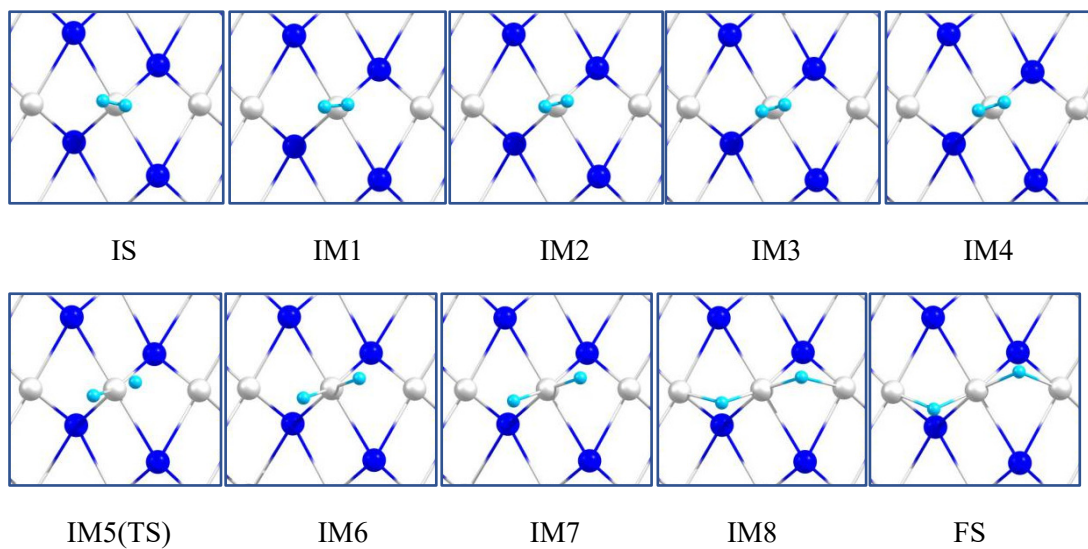|				
IS	IM1	IM2	IM3	IM4
IM5(TS)	IM6	IM7	IM8	FS

Figure S11. Calculated molecular configurations of molecular H_2 over PtSn. Pt in grey, Sn in dark blue atoms, and H in cyan atoms.

REFERENCES

1.   S. H. Joo, J. Y. Park, C. K. Tsung, Y. Yamada, P. Yang and G. A. Somorjai, *Nat. Mater.*, 2009, **8**, 126-131.

2.   R. V. Maligal-Ganesh, C. Xiao, T. W. Goh, L.-L. Wang, J. Gustafson, Y. Pei, Z. Qi, D. D. Johnson, S. Zhang, F. Tao and W. Huang, *ACS Catal.*, 2016, **6**, 1754-1763.

3.   Y. Pei, R. V. Maligal-Ganesh, C. Xiao, T. W. Goh, K. Brashler, J. A. Gustafson and W. Huang, *Nanoscale*, 2015, **7**, 16721-16728.

4.   Y. Pei, B. Zhang, R. V. Maligal-Ganesh, P. J. Naik, T. W. Goh, H. L. MacMurdo, Z. Qi, M. Chen, R. K. Behera, I. I. Slowing and W. Huang, *J. Catal.*, 2019, **374**, 136-142.

5.   Y. C. Pei, Z. Y. Qi, T. W. Goh, L. L. Wang, R. V. Maligal-Ganesh, H. L. MacMurdo, S. R. Zhang, C. X. Xiao, X. L. Li, F. Tao, D. D. Johnson and W. Y. Huang, *Journal of Catalysis*, 2017, **356**, 307-314.

6.   E. W. Zhao, R. Maligal-Ganesh, C. Xiao, T. W. Goh, Z. Qi, Y. Pei, H. E. Hagelin-Weaver, W. Huang and C. R. Bowers, *Angew. Chem. Int. Ed.*, 2017, **56**, 3925-3929.

7.   G. Kresse and J. Furthmüller, *Phys. Rev. B*, 1996, **54**, 11169-11186.

8.   P. E. Blöchl, *Phys. Rev. B*, 1994, **50**, 17953-17979.

9.   J. P. Perdew, K. Burke and M. Ernzerhof, *Phys. Rev. Lett.*, 1996, **77**, 3865-3868.

10.   S. Grimme, J. Antony, S. Ehrlich and H. Krieg, *J. Chem. Phys.*, 2010, **132**, 154104.

11.   H. J. Monkhorst and J. D. Pack, *Phys. Rev. B*, 1976, **13**, 5188-5192.